



Collins, P., & Krauskopf, B. (2002). *Entropy and bifurcations in a chaotic laser*. <http://hdl.handle.net/1983/482>

Early version, also known as pre-print

[Link to publication record in Explore Bristol Research](#)  
PDF-document

## University of Bristol - Explore Bristol Research

### General rights

This document is made available in accordance with publisher policies. Please cite only the published version using the reference above. Full terms of use are available:  
<http://www.bristol.ac.uk/red/research-policy/pure/user-guides/ebr-terms/>

Pieter Collins\*

*Dept of Mathematical Sciences, University of Liverpool, Liverpool L69 7ZL, UK*

Bernd Krauskopf†

*Dept of Engineering Mathematics, University of Bristol, Bristol BS8 1TR, UK*

(Dated: March 21, 2002)

We compute bounds on the topological entropy associated with a transition to chaos via a boundary crisis of the Poincaré return map to a fixed plane of a semiconductor laser with optical injection. Even though this Poincaré map is not defined globally in the whole of the plane, we are still able to compute the stable and unstable manifolds of periodic points globally. In this way, we identify a boundary crisis, which involves periodic point with negative eigenvalues, and obtain the information that forms the input of the entropy calculations. The entropy associated with the chaotic attractor is positive at the boundary crisis and persists in a chaotic saddle after the bifurcation.

## I. INTRODUCTION

Many physical systems exhibit low-dimensional chaotic dynamics. Well-known examples include the Lorenz system [1] and various forced nonlinear oscillators; see Refs. [2] and further references therein. How can one show that a given system is chaotic, or better, determine how chaotic it is? Established methods are the computation of Lyapunov exponents [3] and estimating the fractal dimension of a chaotic attractor [4]. Both methods are computationally expensive and may be inaccurate.

In this paper we show how to compute *rigorous bounds* of the topological entropy [5] by using the methods of trellis theory developed in Refs. [6, 7]. This approach can also be used to extract symbolic dynamics, and it is an example of the study of the dynamics via a topological construction. Other such methods are the Conley index methods of Mischaikow [8] and the topological approximation methods of Rom-Kedar [9]. Topological entropy is a single number measuring how chaotic a given system is, much like a Lyapunov exponent. (There is indeed a deep mathematical connection between the two concepts [10].) While Lyapunov exponents measure how chaotic an individual attractor is, topological entropy is a *global measure* of chaos, and is associated with homoclinic and heteroclinic tangles formed by the stable and unstable manifolds of saddle periodic orbits. For low-dimensional systems, the topological entropy measures the growth rate of the number of hyperbolic periodic orbits, another natural measure of the complexity of the system; see Ref. [11] for this approach.

To showcase the power of our method for practical applications we consider the technologically relevant example of a semiconductor laser subject to external optical injection, introduced in Sec. II below. It is known that optical injection produces an enormous variety of different dynamics, including chaos [12–16], and it was recently

considered for chaotic communication schemes [17, 18]. Its bifurcation (or stability) diagram has been studied extensively [16] and excellent agreement was found with experimental measurements [15, 19]. This revealed different routes to regions of chaos in the system, and sudden bifurcations of chaotic attractors [20, 21].

In this paper we consider one such sudden transition, namely a boundary crisis in the case that the stable and unstable manifolds are non-orientable. Note that the term boundary crisis generally refers to a bifurcation in which a chaotic attractor suddenly disappears when it collides with its basin boundary [22]. Boundary crises have been extensively studied, and are well understood when they occur at a homoclinic or heteroclinic tangency of stable and unstable manifolds [23, 24]. However, here we find a boundary crisis where only the closures of the stable and unstable manifolds under consideration intersect. This phenomenon was first described in the orientation-reversing case by Osinga and Feudel [25]. We give the first detailed account of this phenomenon in the orientation-preserving case which is observed in flows. The disappearance of the chaotic attractor also raises the interesting question of what happens to the entropy during the bifurcation.

Our main tool is to consider a Poincaré map in a suitable section. It is an important observation that the Poincaré map of this laser system is only locally well-defined as the  $k$ -th return map to the section. It is not a globally defined invertible and differentiable planar map on the entire section, and this must be seen as the typical situation in applications. We remark that this is different from what one is used to in much studied examples, such as the Hénon [26] and the Ikeda [27] maps, or the Poincaré maps (which are in fact stroboscopic maps) of the forced Van der Pol and Duffing oscillators [2], which all are globally defined planar maps.

Adapting the method in Ref. [30] to this more general setting allows us to compute suitably long pieces of stable and unstable manifolds as input to the topological algorithm in Ref. [6]. In this way, we establish rigorous bounds for the entropy near the boundary crisis. This constitutes a proof that the semiconductor laser with op-

---

\*Electronic address: [pcollins@liv.ac.uk](mailto:pcollins@liv.ac.uk)

†Electronic address: [B.Krauskopf@bristol.ac.uk](mailto:B.Krauskopf@bristol.ac.uk)

tical injection does indeed have chaotic dynamics.

This paper is organised as follows. In Sec. II we introduce the equations of an optically injected semiconductor laser and discuss its Poincaré map. Global bifurcations are explained in detail in Sec. III and the entropy bounds are the topic of Sec. IV. We draw some conclusions and point to future work in Sec. V. Appendix A is a brief exposition in the Hénon map of a boundary crisis involving the closures of stable and unstable manifolds.

## II. SEMICONDUCTOR LASER WITH OPTICAL INJECTION

A semiconductor laser with optical injection is arguably the most accessible laser system showing chaotic dynamics, being modeled very well by the single-mode rate equations

$$\begin{aligned}\dot{E} &= K + \left(\frac{1}{2}(1 + i\alpha)n - i\omega\right)E \\ \dot{n} &= -2\Gamma n - (1 + 2Bn)(|E|^2 - 1)\end{aligned}\quad (1)$$

for the complex electric field  $E$  and the population inversion  $n$  [16]. The main parameters are the injected field strength  $K$  and the detuning  $\omega$  of the injected field from the solitary laser frequency. The parameters  $\alpha$ ,  $B$  and  $\Gamma$  specify material properties of the laser. In particular,  $\alpha$  is the well-known linewidth enhancement factor and for semiconductor lasers it is in the range  $\alpha \in [1, 10]$ . In this paper we set the material laser parameters to the realistic values  $\alpha = 2$ ,  $B = 0.015$  and  $\Gamma = 0.035$ ; see Ref. [16] for further details.

### A. The Poincaré map

To study system (1), we consider the first Poincaré return map  $f$  to a section. This has the advantage of reducing the system to a two-dimensional iterated map, which is easier to visualise and is more amenable to many kinds of analysis. It is usual to consider a Poincaré section which is everywhere transverse to the flow and to which all trajectories return, in which case the resulting map is globally defined, continuous and invertible. Unfortunately, for the semiconductor laser, there is no such global section, so instead we take a natural section  $\Sigma$  for the system, namely the plane  $\Sigma = \{(E, n) : n = 0\}$ , and treat the resulting pathologies appropriately.

If  $p_0$  is a point on  $\Sigma$  such that the trajectory through  $p_0$  has a first return to  $\Sigma$  at a point  $p_1$ , and the flow is transverse to  $\Sigma$  at  $p_0$  and  $p_1$ , then the first return map  $f$  is locally a diffeomorphism at  $p_0$ . On these regions,  $f$  can be treated like any other diffeomorphism and no special theory is required. However, some initial conditions  $p_0$  may lie in the basin of an attractor which does not intersect  $\Sigma$ . Indeed, it may even be that the trajectory through  $p_0$  never returns to  $\Sigma$ . In this case, the

first return map is undefined at  $p_0$ . For initial conditions approaching the boundary of the domain of definition of  $f$ , the return time typically tends to infinity.

A more serious problem is that the first return map  $f$  need not be continuous. In all cases, a discontinuity of the return map is due to a loss of transversality of the flow with the section. Before discussing the various cases, we first examine the behaviour of the flow of system (1) on  $\Sigma$ .

Since  $\Sigma$  is defined by the condition  $n = 0$ , the direction in which the flow crosses  $\Sigma$  is given by the sign of  $\dot{n}$  at  $n = 0$ . From (1) we see that

$$\dot{n}|_{n=0} = 1 - |E|^2 \quad (2)$$

so  $n$  increases through  $\Sigma$  when  $|E| < 1$  and decreases when  $|E| > 1$ . The flow is tangent to  $\Sigma$  precisely on the unit circle  $C$  given by  $|E| = 1$ . For this system, the tangency set is independent of the parameter values. Even though this parameter independence is not typical, we note that the tangency set is one-dimensional, which is the generic case.

On  $C$  we compute

$$\frac{d}{dt}(|E|^2) = 2K\text{Re}(E) \quad (3)$$

so the flow is directed toward the outside of  $C$  for  $\text{Re}(E) > 0$  and inside for  $\text{Re}(E) < 0$ . Locally,  $C$  divides  $\Sigma$  into two pieces,  $\Sigma_1$  and  $\Sigma_2$ , which we can choose so that the vector field is directed from  $\Sigma_1$  to  $\Sigma_2$ . Assuming further the generic case of a quadratic tangency, we see that points in  $\Sigma_1$  return to the section in  $\Sigma_2$  after a time interval which tends to 0 as the starting point approaches  $C$ , whereas points in  $\Sigma_2$  have no local returns to  $\Sigma$ . Therefore,  $C$  is a discontinuity curve of  $f$ , with  $f(p) \approx p$  if  $p$  is in  $\Sigma_1$  and close to  $C$ , but typically  $f(p) \notin C$  for  $p \in C$ .

Despite these discontinuities, the first return map is still invertible, since an inverse is given by reversing the flow direction. There are three generic types of discontinuity, corresponding to a flow line which is tangent to the section  $\Sigma$  at an initial, interior or final point, respectively. In two of these cases, a locally continuous map can be constructed by allowing the number of returns to the section to vary.

The easiest situation is that the tangency occurs at an interior point of the flow line joining two points. Changing the number of intersections with the section by two allows a smooth extension of the return map, as the flow is transverse to the section at the initial and final points. Similarly, when the tangency occurs at the initial point of the flow line, changing the number of intersections with the section by one allows a continuous extension of the return map, though this is not smooth. However, when the tangency occurs at the final point of the flow line, there is no continuous extension. It is possible to change the number of intersections by one and obtain a return map which is close to the original one.

A continuous extension of the return map is known as a *branch* of the return map. These branches are best understood by considering the set

$$\{(p_0, p_1, t) \in \Sigma \times \Sigma \times \mathbf{R} : \Phi_t(p_0) = p_1\}$$

which gives all possible returns. A more detailed discussion of non-globally defined Poincaré maps, which must be regarded typical in applications, is beyond the scope of this paper.

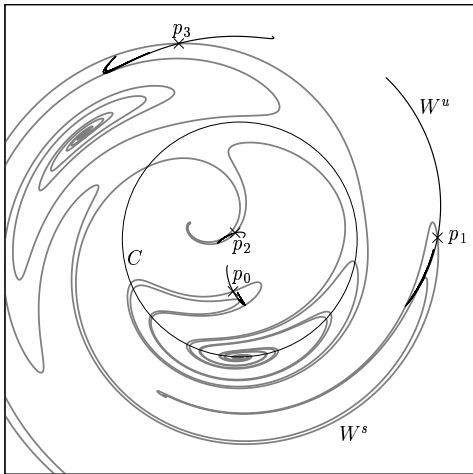


FIG. 1: Stable and unstable manifolds of the 4-periodic points  $\{p_0, p_1, p_2, p_3\}$ , which are in the same orbit under the Poincaré map  $f$ , shown in the section  $\{n = 0\}$  in this and all other figures;  $\omega = 0.270$  and  $K = 0.290$ . On the circle  $C = \{|E| = 1\}$  the Poincaré map is discontinuous.

### B. Stable and unstable manifolds

A great deal of information about the dynamics of the system can be obtained by computing the stable and unstable manifolds of its periodic saddle orbits. For the laser system (1), with parameter values  $K = 0.290$  and  $\omega = 0.270$ , we consider two periodic saddle orbits  $P$  and  $Q$ , with periods 13.14 and 13.19 respectively. The stable and unstable eigenvalues of  $P$  are both positive, and those of  $Q$  are negative, so the invariant manifolds of  $Q$  are non-orientable [29]. We call  $P$  a *direct* saddle orbit and  $Q$  a *flip* (or *twisted*) saddle. The product of stable and unstable eigenvalues for both  $P$  and  $Q$  is less than 1, so both saddles are *dissipative*, that is, the attracting direction is stronger than the repelling one.

Both of these orbits cross the section  $\Sigma$  at four points, which are, therefore, 4-periodic points of the first return map  $f$ . We label these point  $p_0, p_1, p_2, p_3$  and  $q_0, q_1, q_2, q_3$ , where the convention is that the points map to each other in this order and back to  $p_0$  or  $q_0$ , respectively. Figure 1 shows the stable and unstable manifolds of the orbit  $P = \{p_0, p_1, p_2, p_3\}$ .

The stable and unstable manifolds of the  $p_i$ , denoted  $W^s(p_i)$  and  $W^u(p_i)$  respectively, consist of the intersection of the stable and unstable manifolds of  $P$  with the section  $n = 0$ . Since the stable manifold of  $P$  is a smooth surface, its intersection with any section will (generically) consist of an immersed collection of one-manifolds. However, the presence of discontinuities in the first return map means that the properties of the stable manifold may be very different from that of the stable manifold of a surface diffeomorphism. Indeed, we can see that the stable manifolds through  $p_0$  and  $p_3$  and those through  $p_1$  and  $p_2$  coincide. This would be impossible for a diffeomorphism, but can occur here as the stable curve passes through the tangency curve  $C$ . In addition, there are components of the stable manifold which do not contain any of the points  $p_0, p_1, p_2, p_3$ .

The presence of discontinuities complicates the computation of the invariant manifolds. Most algorithms for computing one-dimensional invariant manifolds involve computing the invariant manifold in a neighbourhood of the periodic orbit and growing it. Here we use an adaptation of the algorithm of Krauskopf and Osinga [30], which we combine with the observation that the computation of a continuous branch of the return map can be formulated as a family of boundary value problems. In this way, stable and unstable manifolds can be continued across discontinuities of the first return map by changing the number of iterates. At present we compute the return map by shooting, but one could also use collocation techniques in combination with standard continuation methods, such as is done in the package AUTO [31].

### III. GLOBAL BIFURCATIONS

We now consider the bifurcations of the system as the parameter  $\omega$  is increased from 0.260 to 0.280 keeping  $K$  fixed at 0.290. In this region, sudden bifurcations to chaos have been found in numerically computed bifurcation diagrams, and later also in an experiment on an optically injected DFB laser [19]. Here we consider these transition in much more detail, and this requires looking in a small range for  $\omega$ . The periodic saddle orbits  $P$  and  $Q$  which were computed for  $\omega = 0.270$  can be continued through this parameter range, and they remain direct and flip saddles, respectively.

The first bifurcation we encounter is an *inner tangency* at  $\omega = \omega_{in} \approx 0.269292$ . It is governed by the stable and unstable manifolds of  $P$  and results in the creation of a chaotic saddle. The inner tangency is almost immediately followed by a boundary crisis at  $\omega = \omega_{bc} \approx 0.269299$ . For  $\omega < \omega_{bc}$  the system has a strange attractor  $A$ . In the boundary crisis, this attractor collides with the chaotic saddle and is destroyed. The system then jumps to a periodic attractor.

The boundary crisis is caused by the intersection of the closure of  $W^u(Q)$ , which constitutes the attractor  $A$ , and

the closure of  $W^s(P)$ , which constitutes the boundary of the basin of attraction. For this to happen, we must already have intersections of  $W^u(P)$  and  $W^s(P)$ . Hence, the inner tangency is a vital ingredient in the destruction of the strange attractor. However, the bifurcations occur very close together in the injected laser, which makes it difficult to distinguish them.

A boundary crisis of flip saddles, involving the closures of the stable and unstable manifolds, has not been described in detail. It was discussed in Ref. [25] in the orientation-reversing case. In Appendix A we illustrate this global bifurcation and its effects  $W^u(Q)$  in the orientation-preserving Hénon map. This has the additional advantage, that there is no inner tangency close to the boundary crisis.

A description of the bifurcations can be obtained by considering the Poincaré return map to  $\Sigma$ . As  $\omega$  varies,  $P$  and  $Q$  each continue to intersect  $\Sigma$  transversely at four points. The strange attractor  $A$  intersects  $\Sigma$  in four components,  $A_0, A_1, A_2, A_3$ , with each  $A_i$  containing  $q_i$  and being invariant under  $f^4$ . The component  $A_0$  is contained in the rectangle  $R = [-0.1, -0.2] \times [-0.65, 0.35]$ . Although  $f$ , and hence  $f^4$  are not globally continuous, the restriction of  $f^4$  to  $R$  is, so the dynamics on this set is essentially that of a diffeomorphism, and is governed by the two periodic saddle points  $p_0$  and  $q_0$  and their stable and unstable manifolds.

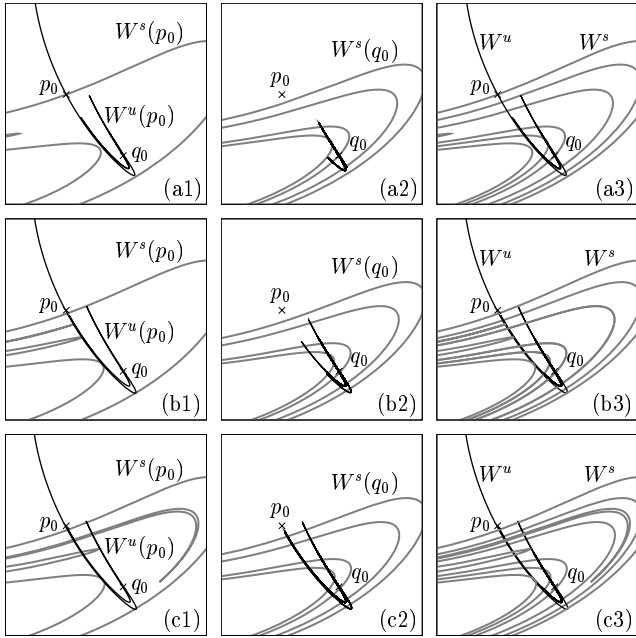


FIG. 2: Stable and unstable manifolds of the 4-periodic point  $p_0$  (left column), of the 4-periodic point  $q_0$  (middle column), and of both  $p_0$  and  $q_0$  (right column), before (row a), approximately at (row b) and after (row c) the destruction of a chaotic attractor;  $K = 0.290$  and from (a) to (c)  $\omega = 0.2673, 0.269292, 0.270$ .

## A. Inner tangency

For parameter values of  $\omega$  less than  $\omega_{\text{in}}$ , the geometry of the stable and unstable manifolds of  $p_0$  and  $q_0$  is as shown in the first column of Fig. 2. The closure of the unstable manifold of the flip saddle  $q_0$  is a chaotic attractor  $A_0$  with a positive Lyapunov exponent and positive entropy. For many parameter values, this attractor may have smaller sub-attractors inside it, including stable periodic orbits [32], but the observable behaviour is that of a single strange attractor. One branch of the unstable manifold of  $p_0$  ends in a periodic attractor  $r_0$ , and the other branch intersects the stable manifold of  $q_0$ . Hence, points near  $p_0$  are either attracted to  $A_0$  or to  $r_0$ . The stable manifold of  $p_0$  does not intersect the unstable manifold of  $p_0$ , so there are no orbits homoclinic to  $p_0$ .

The stable and unstable manifolds to  $p_0$  at the inner tangency bifurcation occurring for  $\omega = \omega_{\text{in}}$ , are shown in Fig. 2 (b1). The attractor  $A_0$  persists, but there is now a new basic set associated with the homoclinic orbits to  $p_0$ , also with positive topological entropy. Since the direct saddle  $p_0$  is dissipative, a result of Palis and Takens [33] shows that there must have been chaotic attractors present near  $p_0$  even before this bifurcation, but these are small enough not to be physically relevant. The significance of this bifurcation is that now there are no topological obstructions for the stable manifold of  $p_0$  to intersect the unstable manifold of  $q_0$ .

Because  $Q$  is a flip saddle, there can be no parameter value at which a first tangency of  $W^s(P)$  and  $W^u(Q)$  exists. Instead it is characterised by the intersection of the closures of  $W^s(P)$  and  $W^u(Q)$ . Indeed, the closures of these manifolds appear to intersect tangentially giving a *closure heteroclinic tangency* in the terminology of [25]. In this bifurcation the chaotic attractor  $A$  collides with the chaotic saddle that was created in the inner tangency.

## B. Boundary crisis involving flip saddle

The attractor  $A$  is destroyed in the boundary crisis occurring at  $\omega = \omega_{\text{bc}}$ , soon after the inner tangency. For  $\omega < \omega_{\text{bc}}$ , the stable manifold of  $p_0$ ,  $W^s(p_0)$ , and the unstable manifold of  $q_0$ ,  $W^u(q_0)$ , are disjoint, and we have a strange attractor consisting of the closure of the unstable manifold of  $q_0$ ,  $\overline{W^u(q_0)}$ . For  $\omega > \omega_{\text{bc}}$ , the manifolds  $W^s(p_0)$  and  $W^u(q_0)$  intersect transversely, and we now have a heteroclinic tangle formed by the stable and unstable manifolds of  $p_0$  and  $q_0$ . Therefore  $\overline{W^u(q_0)}$  and  $\overline{W^u(p_0)}$  are the same, and the closure of the unstable manifold  $W^u(q_0)$  is no longer a strange attractor. Instead, almost every point is attracted to the periodic point  $r_0$ . This bifurcation gives a *discontinuous* change in the closure of  $W^u(q_0)$ .

As  $\omega$  approaches  $\omega_{\text{bc}}$  from above, there are infinitely many parameter values at which heteroclinic tangencies of  $W^s(p_0)$  and  $W^u(q_0)$  occur, and  $\omega_{\text{bc}}$  is a limit point of these values. Since  $q_0$  is a flip saddle, its unstable mani-

fold limits on itself from both sides, so it can never have tangencies with any stable manifold without also having transverse crossings. At  $\omega_{bc}$ , the manifolds  $W^s(p_0)$  and  $W^u(q_0)$  must still be disjoint, but they do have common limit points. Therefore, we call this bifurcation a *limit crisis*. Thus at the limit crisis, the closures of the manifolds,  $\overline{W^s(p_0)}$  and  $\overline{W^u(q_0)}$ , intersect, and numerical evidence strongly suggests that  $\overline{W^s(p_0)}$  and  $\overline{W^u(q_0)}$  are tangent at the bifurcation giving a *closure heteroclinic tangency* [25]. Although  $W^s(p_0)$  and  $W^u(q_0)$  are disjoint, there may be periodic saddle points in  $\overline{W^s(p_0)}$  and  $\overline{W^u(q_0)}$  whose unstable manifolds do have a first tangency at  $\omega_{bc}$ , in which case the crisis is as described in [22].

The limit crisis can be seen as a bifurcation of the chaotic saddle  $B$  associated with the homoclinic tangle of  $P$  and the attractor  $A$  associated with the homoclinic tangle of  $Q$ ; see Appendix A. A natural consequence is that at the boundary crisis, the topological entropy associated with  $A$  and  $B$  must be the same; see also Section IV.

#### IV. TOPOLOGICAL ENTROPY

As mentioned in the introduction, topological entropy is a global measure of the degree of chaos of a dynamical system, and is associated with the growth rate of the number of periodic points of a given period. There is also a notion of entropy applied to a homoclinic or heteroclinic tangle, which is given in terms of the growth rate of the number of intersections of initial branches of stable and unstable manifold under iteration of the latter. The entropy of a tangle is equal to the growth rate of the periodic orbits associated with the tangle. Since some entropy may be associated with other tangles of the system, the entropy of the tangle under consideration is a lower bound for the topological entropy of the system.

Here, we estimate the topological entropy of the fourth return map of the semiconductor laser using the methods described in [6, 7] and also give a detailed description of the system in terms of symbolic dynamics. For the remainder of this section, we shall use  $\tilde{f}$  to refer to the fourth return map  $f^4$  of the laser system.

The quality of the information obtained depends greatly upon the length of stable and the unstable manifolds one computes. Consider the initial pieces of stable and unstable manifold, called a *trellis*, shown in Figure 3(a). The stable and unstable manifolds are such that no information about the entropy can be obtained other than the standard result that it must be strictly positive.

In Fig. 3(b), the trellis divides  $\Sigma$  into a number of regions. It can be shown that the regions  $R_A$  and  $R_B$  must contain chaotic dynamics. Orbits that are entirely contained in these two regions can be coded symbolically by assigning to each orbit the sequence of  $A$ 's and  $B$ 's such that the  $k^{\text{th}}$  element of the sequence gives the region

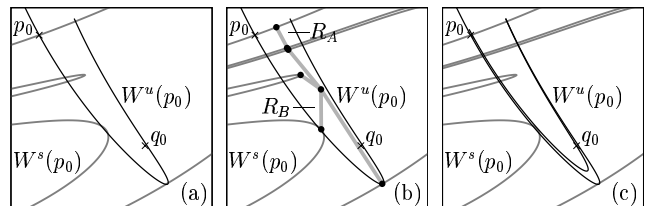


FIG. 3: Initial branches of stable and unstable manifolds of  $p_0$  from Fig. 2 form a trellis that does not force chaotic dynamics (a). For a longer piece of  $W^s(p)$  the trellis bounds two regions  $R_A$  and  $R_B$  with positive entropy dynamics (b), while an even longer piece of  $W^s(p)$  reveals that the regions of chaotic dynamics are thin strips (c);  $K = 0.290$  and  $\omega = 0.270$ .

containing the  $k^{\text{th}}$  iterate. Such a sequence is called an *itinerary* of the point. Using our methods, we can show that  $\tilde{f}$  must have orbits of every itinerary except those which contain a word of the form  $AB^{4n+k}A$  where  $k = 1$  or  $k = 2$ ; see below for more details.

Increasing the length of stable and computed unstable manifolds allows better estimates of the symbolic dynamics, and better entropy bounds can be obtained. The unstable curve shown in Fig. 3(c) is the iterate of that shown in Fig. 3(b). We can now deduce that the chaotic saddle which must exist in regions  $R_A$  and  $R_B$ , must lie in the very thin strip bounded by the indicated piece of  $W^u(p_0)$ .

We now return to consider the trellis for  $\omega = 0.270$  of Fig. 3(b) in more detail. The symbolic dynamics is found by constructing a graph  $G$  embedded in the complement of the unstable manifold, and using the stable manifold to induce an action  $g$  on this graph; see Fig. 4. The edges of  $G$  are of two types, *control edges*, shown in black, and *expanding edges*, shown in gray. The control edges are short edges crossing the stable manifold. Their primary role is to capture the topological and dynamical information contained in the stable manifold. The expanding edges connect the control edges without crossing the trellis or introducing unnecessary loops. They carry all the interesting dynamical information.

Performing the algorithm given in [6] we obtained the graph in Fig. 4. The induced action  $g$  on the expanding edges of the graph is given by

$$a \mapsto ab_1\bar{b}_2, \quad b_1 \mapsto b_2, \quad b_2 \mapsto b_3, \quad b_3 \mapsto b_4, \quad b_4 \mapsto ab_1. \quad (4)$$

We see that orbits of  $g$  also have an itinerary given by  $A$ 's and  $B$ 's, with the edge  $a$  corresponding to  $A$ , and the edges  $b_1, b_2, b_3$  and  $b_4$  corresponding to  $B$ .

The most important property of  $g$  is that for any orbit of  $g$ , there is an orbit of  $\tilde{f}$  with the same itinerary. The orbits of  $g$  are said to *force* orbits of  $\tilde{f}$ . Furthermore, for any periodic orbit of  $g$ , there is a periodic orbit of  $\tilde{f}$  with the same itinerary and period. For example, the 4-periodic orbit of  $g$  that visits edges  $a, b_2, b_3$  and  $b_4$

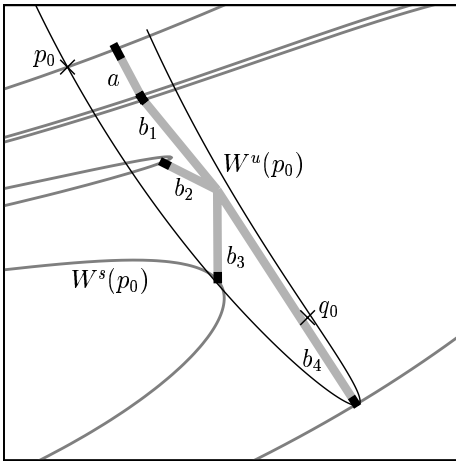


FIG. 4: Initial branches of stable and unstable manifolds of  $p_0$  from Fig. 3(b), with a corresponding graph  $G$  capturing the topology of the trellis;  $K = 0.290$  and  $\omega = 0.270$ .

forces a 4-periodic orbit of  $\tilde{f}$  with itinerary  $(ABBB)^{\mathbb{Z}}$ . We can also deduce information about the orbits of  $A$  that are homoclinic to  $p_0$ : for any orbit of  $g$  that has all but finitely many points in  $a$  (and so whose itinerary is homoclinic to  $A^{\mathbb{Z}}$ ), there is a corresponding orbit of  $\tilde{f}$  which is homoclinic to  $p_0$ .

The converse of these forcing results is not true; the orbits of  $\tilde{f}$  do not force orbits of  $g$ , and in many cases there *must* be orbits of  $\tilde{f}$  that have a different itinerary from any orbit of  $g$ . Therefore, all we can say is that the dynamics of  $\tilde{f}$  are more complicated than those of  $g$ . This is well-reflected in the topological entropy, which satisfies the inequality

$$h_{top}(\tilde{f}) \geq h_{top}(g) \quad (5)$$

For this example of  $\omega = 0.270$ , we find  $h_{top}(g) \approx \log(1.544) \approx 0.434$ , giving a lower bound for the entropy of the system as  $h_{top}f^4 \geq 0.434$ .

$\omega$	$\omega_{\text{lim}} \approx 0.269292$	0.278	0.280	0.282
$h_{top}(\tilde{f})$	0.436	0.596	0.596	$\log 2 \approx 0.693$

TABLE I: Lower estimates of the topological entropy of  $\tilde{f} = f^4$ ;  $K = 0.290$  and  $\omega$  is as indicated.

We now study how the topological entropy changes with the parameter  $\omega$ ; the resulting estimates for the entropy are summarized in Table I. For  $\omega < \omega_{bc}$ , the topological entropy of the attractor  $A_0$  can be estimated by considering the trellis formed by the stable and unstable manifolds of  $q_0$ . Since the stable manifold of  $p_0$  and the unstable manifold of  $q_0$  do not intersect, the dynamics on the attractor can be considered separately from that

of the chaotic saddle associated with  $p_0$ . For the stable and unstable manifolds of  $q_0$  computed for both  $\omega = \omega_{in}$  and  $\omega = \omega_{bc}$ , the bound for the entropy of the attractor is 0.346, though the actual entropy may increase slightly. At  $\omega = \omega_{in}$ , the entropy of the trellis associated with  $p_0$  is 0, and at the limit bifurcation, the entropy of the trellises associated with  $p_0$  and  $q_0$  must be equal, hence the entropy of the trellis associated with  $p_0$  must be at least 0.346.

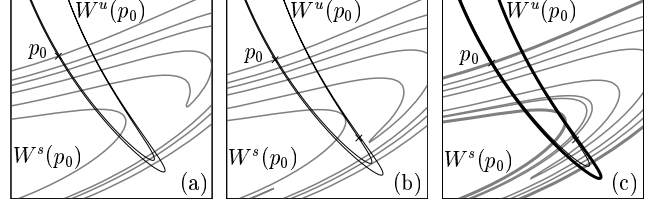


FIG. 5: The emergence of a full horseshoe of  $f^4$ ;  $K = 0.290$  and from (a) to (c)  $\omega = 0.278, 0.280, 0.282$ .

As  $\omega$  increases further, more intersections of stable and unstable manifold are created. While some of the fine structure of the tangle may change for  $\omega$  between 0.272 and 0.280, there are no significant changes. For  $\omega$  between 0.280 and 0.282, there is a bifurcation sequence, illustrated in Fig. 5, which ends in the creation of a full Smale horseshoe. The entropy bound for the chaotic saddle increases, and appears to change continuously with  $\omega$ , though the bound computed from given finite pieces of stable and unstable manifold jumps at the homoclinic tangencies. For the trellises in Fig. 5, we compute entropy bounds of 0.596, 0.596 and  $\log 2 \approx 0.693$ , respectively; see also Table I. However, this entropy only measures the complexity of the transient orbits, and would not be seen if the system was already locked to the stable limit cycle  $r_0$ ; see Sec. II. It is a curious phenomenon that the entropy of the chaotic set is increasing as  $\omega$  increases past the limit bifurcation. In other words, while the *complexity* of the system as measured by the topological entropy is increasing, the *observed* behaviour becomes simpler, because the chaotic set loses stability and only  $r_0$  remains as an attractor.

## V. CONCLUSIONS

The method of analysis presented here can be extended to any low-dimensional system. We have seen that invariant curves of saddle points in a section can be computed even if there is no globally defined, continuous return map. From these manifolds, the structure of the large-scale attractors of the system can be computed, and bifurcations in which they are destroyed can also be found.

One can then compute good lower bounds for the topological entropy on attractors and chaotic non-attracting

sets, and obtain a description of their internal dynamics in terms of the itineraries.

For the laser system described, there is a bifurcation sequence in which an inner tangency of a direct saddle is a prerequisite for the disappearance at a boundary crisis of a chaotic attractor, which is the closure of the unstable manifold of a flip saddle. This bifurcation sequence is typical in two-dimensional orientation-preserving diffeomorphisms and three-dimensional flows, as was demonstrated by identifying this type of boundary crisis also in the Hénon map. At the boundary crisis the entropy associated with the chaotic attractor is positive, and it persists as the entropy associated with a chaotic saddle after the bifurcation.

### Acknowledgements

The authors thank Hinke Osinga for valuable input concerning the literature on crisis bifurcations and Sebastian Wicczorek for helpful discussions. The research of P.C. was supported by a Leverhulme Special Research Fellowship, and that of B.K. by an EPSRC Advanced Research Fellowship.

## APPENDIX A: BOUNDARY CRISIS IN THE HÉNON MAP

The scenario described above, in which a limit crisis is responsible for the destruction of a strange attractor, is typical in orientation-preserving diffeomorphisms, which include all return maps of flows. Indeed, this bifurcation is responsible for the destruction of a strange attractor in the Hénon map

$$H(x, y) = H_{a,b}(x, y) = (a - x^2 - by, x) \quad (\text{A1})$$

in the orientation-preserving case  $b > 0$ ; see [34] for an example. We fix  $b = 0.5$ , so  $H$  is uniformly dissipative, and vary the parameter  $a$ .

For sufficiently large  $a$ ,  $H$  has two saddle fixed points, a direct saddle  $p$  and a flip saddle  $q$ , which means that we are in the same situation as discussed previously for the injected laser. For  $a > 0.840$  the manifolds  $W^u(p)$  and  $W^s(p)$  intersect transversely yielding homoclinic orbits to  $p$ . For parameter value  $a = 2.4$ ,  $W^u(p)$  intersects both  $W^s(p)$  and  $W^s(q)$ , but  $W^u(q)$  does not intersect  $W^s(p)$ , as shown in Fig. 6(a). The closure of  $W^u(q)$  is a strange attractor  $A$ , and remains inside a region bounded by an arc of  $W^u(p)$  and an arc of  $W^s(p)$ . The boundary of the basin of attraction of  $A$  is  $\overline{W^s(p)}$ .

For  $a = 2.5$ , shown in Fig. 6(b), the situation is very different.  $W^u(q)$  now intersects  $W^s(p)$ . Since points

which lie to the left of  $W^s(p)$  escape to infinity, there is an open set in  $\overline{W^u(q)}$  consisting of points which escape to infinity, and the set of points which escape is dense. The closure of the set of points heteroclinic to  $p$

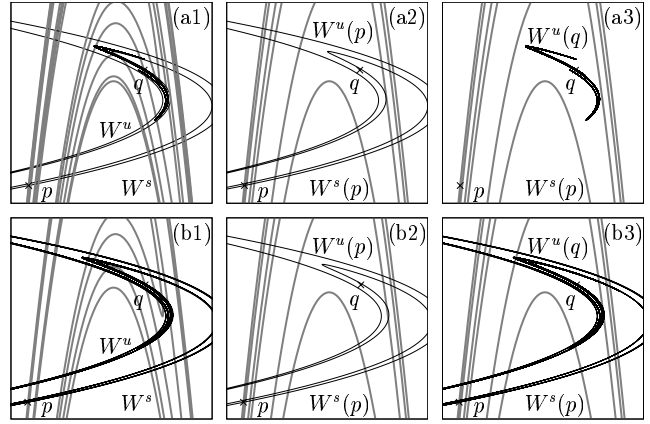


FIG. 6: Before (row a) and after (row b) a limit bifurcation in the Hénon map. Shown are the stable and unstable manifolds of  $p$  and  $q$  (left column), just of  $p$  (middle column), and the stable manifold of  $p$  and unstable manifold of  $q$  (right column);  $b = 0.5$ , and  $a = 2.4$  (row a) and  $a = 2.5$  (row b).

and  $q$  is now a chaotic saddle, and gives only transient behaviour of the map; all other points escape to infinity.

Once  $W^s(p)$  and  $W^u(q)$  intersect, they must do so arbitrarily close to  $p$ , and, by the  $\lambda$ -lemma [35], the closure of  $W^u(p)$  contains  $W^u(q)$ . Hence,  $W^u(p)$  and  $W^u(q)$  have the same closures. This means that the branches of  $W^u(q)$  now limits on the branch of  $W^s(U)$  which extends to infinity. Hence, this type of boundary crisis is a discontinuity point of  $\overline{W^u(q)}$  (using the Hausdorff metric on sets).

To illustrate this, in Fig. 7 we show how  $W^u(q)$  is build up in successive iterates. In Fig. 7(row a), we have computed  $W^u(q)$  to length 1; successive figures are computed by iterating the unstable curve. Notice how for the first few iterates, the unstable curve remains close to the former attractor, but as higher iterates are computed, there are arcs that cross  $W^s(p)$  closer and closer to  $p$ . Although the topology of the unstable manifold changes discontinuously at the limit bifurcation, for parameter values close to the induced boundary crisis, a very large number of iterates of the initial segment of unstable manifold are needed to cross a given arc in  $W^s(p)$ . This must be the case, since even though the topology of the manifold can change discontinuously, any fixed iterate must change continuously.

[1] E. N. Lorenz, J. Atmos. Sci. **20**, 130 (1963).

[2] J. Guckenheimer and P. Holmes, *Nonlinear Oscillations*,



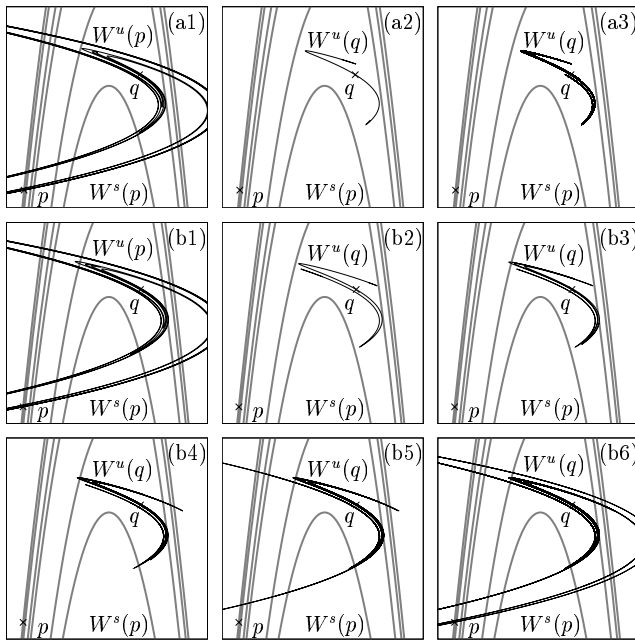


FIG. 7: The manifold  $W^u(p)$  changes little in the limit bifurcation, see (a1) and (b1), but  $W^u(q)$  changes dramatically. Before the limit bifurcation longer and longer pieces of  $W^u(q)$  in panels (a2) and (a3) stay bounded, while after the limit bifurcation longer and longer pieces of  $W^u(q)$  in panels (b2) to (b6) converge to  $W^u(p)$ . Close to the limit bifurcation one needs to compute very long pieces of  $W^u(q)$  to see its convergence to  $W^u(p)$ ;  $b = 0.5$ , and  $a = 2.4$  (row a) and  $a = 2.5$  (rows b).

*Dynamical Systems, and Bifurcations of Vector Fields*, no. 42 in Applied Mathematical Sciences (Springer-Verlag, 1983).

- [3] J. B. Pesin, *Russ. Math. Surv.* **32**, 55 (1977).
- [4] P. Grassberger, in *Chaos* (Manchester University Press, 1986), pp. 291.
- [5] R. Bowen, in *Global Analysis* (1970), no. 14 in Proceedings of Symposia in Pure Mathematics, pp. 23.
- [6] P. Collins (2001), "Symbolic dynamics from homoclinic tangles", *Intern. J. Bifur. Chaos*, to appear.
- [7] P. Collins, in *Geometry and Topology in Dynamics*, edited by M. Barge and K. Kuperberg (American Mathematical Society, 1999), no. 246 in Contemporary Mathematics.
- [8] K. Mischaikow, in *Dynamical Systems*, edited by R. Johnson (Springer, Berlin, 1997), no. 1609 in Lecture Notes In Mathematics, pp. 119.
- [9] V. Rom-Kedar, *Nonlinearity* **7**, 441 (1994).

- [10] M. Misiurewicz, *Astérisque* **40**, 147 (1976).
- [11] R. L. Davidchack and Y.-C. Lai, *Phys. Rev. E* **60**(1999) 6172.
- [12] L. A. Lugiato, L. M. Narducci, D. K. Bandy, and C. A. Pennise, *Opt. Comm.* **46**, 64 (1983).
- [13] J. R. Tredicce, F. T. Arecchi, G. L. Lippi, and G. Puc-cioni, *J. Opt. Soc. Am. B* **2**, 173 (1985).
- [14] V. Kovanis, A. Gavrielides, T. Simpson, and J. Liu, *Appl. Phys. Lett.* **67**, 2780 (1995).
- [15] T. B. Simpson, J. M. Liu, K. F. Huang, and K. Tai, *Quant. Semiclass. Opt.* **9**, 765 (1997).
- [16] S. M. Wieczorek, B. Krauskopf, and D. Lenstra, *Opt. Comm.* **172**, 279 (1999).
- [17] V. Annovazzi-Lodi, S. Donati, and A. Scire, *J. Quantum Electron.* **32**, 953 (1996).
- [18] H. F. Chen and J. M. Liu, *J. Quantum Electron.* **36**, 27 (2000).
- [19] S. Wieczorek, T. B. Simpson, B. Krauskopf, and D. Lenstra, Global quantitative predictions of complex laser dynamics, *Phys. Rev. E* R15204 (2002), to appear.
- [20] B. Krauskopf, S. M. Wieczorek, and D. Lenstra, *Appl. Phys. Lett.* **77**, 1611 (2000).
- [21] S. M. Wieczorek, B. Krauskopf, and D. Lenstra, *Opt. Lett.* **26**, 816 (2001).
- [22] C. Grebogi, E. Ott, and J. A. Yorke, *Physica D* **7**, 181 (1983).
- [23] C. Grebogi, E. Ott, and J. A. Yorke, *Physica D* **7**, 243 (1987).
- [24] C. Robert, K.T. Alligood, E. Ott, and J.A. Yorke, *Physica D* **144**, 44 (2000).
- [25] H. Osinga and U. Feudel, *Physica D* **141**, 54 (2000).
- [26] M. Hénon, *Comm. Math. Phys.* **50**, 69 (1976).
- [27] K. Ikeda, *Opt. Communications* **30**, 257 (1979);
- [28] S. M. Hammel, K.R.T. Jones, and J. Moloney, *J. Opt. Soc. Am. B* **2**, 552 (1985).
- [29] H. Osinga "Nonorientable manifolds of three-dimensional vector fields" (2001), University of Bristol ANM-Preprint **2001.15**.
- [30] B. Krauskopf and H. Osinga, *J. Comput. Phys.* **146**, 404 (1998).
- [31] J. Guckenheimer, E. J. Doedel, A. R. Champneys, T. F. Fairgrieve, Yuri A. Kuznetsov, B. Sandstede, and X. J. Wang *AUTO97: Continuation and bifurcation software for ordinary differential equations*.
- [32] S. E. Newhouse, in *Dynamical Systems (C.I.M.E. Summer School, Bressanone, 1978)* (Birkhäuser, 1980), vol. 8 of *Progress in Mathematics*, pp. 1–114.
- [33] J. Palis and F. Takens, *Hyperbolicity and sensitive chaotic dynamics at homoclinic bifurcations*, no. 35 in Cambridge Studies in Advanced Mathematics (Cambridge University Press, 1993).
- [34] J. Gallas, C. Grebogi, and J. A. Yorke, *Phys. Rev. Lett.* **71**, 1359 (1993).
- [35] J. Palis, *Topology* **8**, 385 (1969).